MORPHOLOGICAL GRADIENTS BASED ON NEIGHBORHOOD-CONTROLLED FUZZY ROUGH APPROXIMATIONS: A COMPARATIVE VISUALIZATION STUDY

Mădălina Roxana Buneci, Associate Professor

"Constantin Brâncuși" University from Târgu Jiu, ROMANIA

ABSTRACT: *Building on the fact that the neighborhood-controlled fuzzy upper and lower rough approximation operators [X. Han, W. Yao, C.-J. Zhou, Topology and its Applications, 2025)] form a pair of extensive and anti-extensive transforms, we introduce new variants of the morphological gradient based on these fuzzy rough approximations. To empirically evaluate their performance, we employ a comparative visualization methodology centered on the superposition of resulting gradient images, allowing for an intuitive and direct comparison of edge detection capabilities and noise sensitivity. For the purpose of this study, we developed a dedicated software framework in the C programming language. Pixel-level image manipulation and visualization are facilitated by the SDL3 library.*

KEY WORDS: *fuzzy upper rough approximations, fuzzy lower rough approximations, morphological gradient*.

1. INTRODUCTION

Edge detection continues to be a fundamental pillar of image analysis, providing crucial information for segmentation, recognition, and feature extraction tasks [8]. Among the numerous techniques developed, morphological gradients, derived from the principles of mathematical morphology, offer a robust, non-linear alternative to differential methods by emphasizing geometrical and topological properties of images rather than local intensity derivatives (see [5], [7]).

The classical morphological gradient, defined as the difference between the dilation and erosion of an image by a structuring element, has proven effective in highlighting transitions in intensity while maintaining resilience to small-scale noise. Despite its success, the traditional morphological gradient may not optimally capture subtle variations in texture or contrast, nor does it always yield edge representations well-suited for subsequent segmentation. For this reason, numerous extensions and variants have been proposed, such as internal and external gradients, regularized gradients (see [5], [1]) and multiscale morphological operators, to improve localization, continuity, and robustness. Nevertheless, there remains a need for systematic exploration of alternative formulations that can better balance sensitivity to fine details with resistance to noise and scale variations.

In this paper, we introduce several new variants of the morphological gradient based on fuzzy rough sets (specifically, on neighborhood-controlled fuzzy upper and lower rough approximation operators [2]). Each variant is formulated by modifying the morphological operations or their combination, yielding distinct gradient responses.

To evaluate the performance and characteristics of these new operators, we propose a comparative visualization method based on the superposition of the resulting gradient images. Specifically, for each input image, the new gradient and the classical

gradient are computed and overlaid; points where the two coincide are highlighted with a distinct color. This visual correspondence provides an intuitive means of assessing the similarity, complementarity, or divergence between the proposed variants and the standard morphological gradient. Through this comparison, we aim to identify which modifications preserve essential edge information, which yield additional or refined contours, and which suppress spurious responses.

2. NEIGHBORHOOD-CONTROLLED FUZZY ROUGH APPROXIMATION OPERATORS AND GRADIENTS

A hemimetric on a space X is a function

$$d : X \times X \to [0, \infty)$$

satisfying the conditions:

1) $d(x, x) = 0$ for all $x \in X$.

2) $d(x, z) \le d(x, y) + d(y, z)$ for all $x, y, z \in X$.

Let X be endowed with a preorder ρ (i.e. a reflexive and transitive relation). If

$$d: X \times X \to [0, \infty)$$

is a hemimetric on X with the property that there is $c \in \mathbb{R}$ such that that $d(x, y) \le c$ for all $x, y \in X$, then

$$d_\rho : X \times X \to [0, \infty),$$

defined by

$$d_\rho(x, y) = \begin{cases} d(x, y), & \text{if } x \rho y \\ c, & \text{otherwise} \end{cases}$$

is a hemimetric. Indeed, let $x, y, z \in X$. We write $a \not\rho b$ if not ($a \rho b$). If $x \rho z$, then

$$d_\rho(x, z) = d(x, z) \le d(x, y) + d(y, z) \le \le d_\rho(x, y) + d_\rho(y, z).$$

If $x \not\rho z$, then $x \not\rho y$ or $y \not\rho z$. Consequently, $d_\rho(x, y) = c$ or $d_\rho(y, z) = c$. Therefore,

$$d_\rho(x, z) = c \le d_\rho(x, y) + d_\rho(y, z).$$

Let us consider a hemimetric d on a space X and as in [ha] let us denote by

$$\mathcal{F}(X) = \{ \omega: X \to \mathbb{R}\}$$

the fuzzy subsets of X ($\mathbb{R}$ is the field of all real numbers). Also, for $x \in X$ and $r > 0$, let us denote by

$$L_r(x) = \{s \in X | \ d(s, x) < r\}$$
$$R_r(x) = \{s \in X | \ d(x, s) < r\},$$

the left r-neighborhood and the right r-neighborhood of x [2]. If d is a metric, or more general a pseudometric, then $L_r(x) = R_r(x) = B(x, r)$ (the open ball of radius r). But if d is not symmetric, then $L_r(x)$ and $R_r(x)$ does not necessarily coincide. For instance, let us consider X be a bounded subset of $\mathbb{R}^2$ and let d_2 be the Euclidian metric on restricted to X. Let $c \in \mathbb{R}$ be such that

$$c > \text{diam}(X) = \sup\{d_2(p, q) | \ p, q \in X\}$$

and as above for a preorder ρ on X, let us consider the hemimetric $d_{2\rho}$ defined by

$$d_{2\rho}(p, q) = \begin{cases} d_2(p, q), & \text{if } p \rho q \\ c, & \text{otherwise} \end{cases}$$

Let's graphically represent the left r-neighborhood $L_r(p)$ (colored in blue) and the right r-neighborhood $R_r(p)$ (colored in green) of a point p (colored in red) for the following preorders on $X \subset \mathbb{R}^2$:

1. $(x_1, y_1)\ \rho_1\ (x_2, y_2)$ iff $x_1 \le x_2$ and $y_1 \le y_2$
2. $(x_1, y_1)\ \rho_2\ (x_2, y_2)$ iff $x_1 \le x_2$
3. $(x_1, y_1)\ \rho_3\ (x_2, y_2)$ iff $x_1 \le x_2$ and $y_1 = y_2$

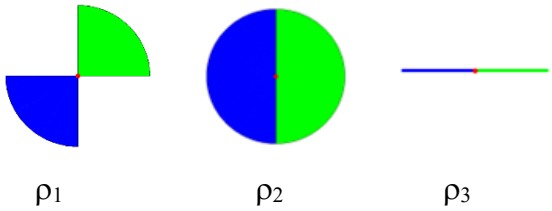

ρ_1 ρ_2 ρ_3

Figure 1. Left/right neighborhoods with respect to $d_{2\rho_i}$, i = 1, 2, 3

In [2], the authors defined neighborhood-controlled fuzzy upper rough approximation operators on X and lower rough approximation operators on X with respect to the radius r induced by the hemimetric d

$$\overline{\text{App}}^r, \underline{\text{App}}^r : \mathcal{F}(X) \to \mathcal{F}(X)$$

defined by

$$\overline{\text{App}}^r(\omega)(x) = \sup\{\omega(s) - d(s, x) | \ s \in L_r(x)\}$$
$$\underline{\text{App}}^r(\omega)(x) = \inf\{\omega(s) + d(x, s) | \ s \in R_r(x)\}$$

for all $x \in X$ and $\omega \in \mathcal{F}(X)$, where

In [2] the r-closing operator is defined as the composition of upper-lower operators

$$\underline{\text{App}}^r \circ \overline{\text{App}}^r,$$

and the r-opening operator as the composition of lower-upper operators

$$\overline{\text{App}}^r \circ \underline{\text{App}}^r,$$

For r = + ∞, the operators $\overline{\text{App}}^{r}$ and $\underline{\text{App}}^{r}$ become the operators introduced in [9]. A convex combination

$$\lambda\underline{\text{App}}^{\infty}(\omega) + (1-\lambda)\overline{\text{App}}^{\infty}(\omega),$$

for a suitable λ, was used in [9] to find a contour which is nearest to the digital surface ω. There are subtle distinctions among the terms "edge," "boundary," and "contour," as they are primarily conceptual notions rooted in experience rather than precise mathematical definitions [8]. For a brief explanation of their differences, see, for example, [8].

A morphological gradient is the difference between an extensive and an anti-extensive transformation [5]. An operator

$$\Phi: \mathcal{F}(X) \to \mathcal{F}(X)$$

is said to be extensive if $\omega \leq \Phi(\omega)$ for all $\omega \in \mathcal{F}(X)$. An operator

$$\Psi: \mathcal{F}(X) \to \mathcal{F}(X)$$

is said to be anti-extensive if $\Psi(\omega) \leq \omega$ for all $\omega \in \mathcal{F}(X)$. Since d(x, x) = 0, it follows that for all r > 0, we have

$$\underline{\text{App}}^{r}(\omega)(x) \leq \omega(x) \leq \overline{\text{App}}^{r}(\omega)(x).$$

Hence $\underline{\text{App}}^{r}$ is anti-extensive and $\overline{\text{App}}^{r}$ is extensive. Based on these observations we define the following versions of morphological gradients with respect to a fixed hemimetric d:

symmetric morphological gradient

$$g_r(\omega) = \overline{\text{App}}^{r}(\omega) - \underline{\text{App}}^{r}(\omega)$$

internal morphological gradient

$$g_r^{-}(\omega) = \omega - \underline{\text{App}}^{r}(\omega)$$

external morphological gradient

$$g_r^{+}(\omega) = \overline{\text{App}}^{r}(\omega) - \omega$$

ω_i $g_r(\omega_i)$ $g_r^{-}(\omega_i)$ $g_r^{+}(\omega_i)$

Figure 2. Inverted morphological gradients based on rough approximations

Figure 2 illustrates the morphological gradients in the aforementioned context for the standard Lenna image rendered in grayscale in two variants. The first variant ω_1 employs luminance, calculated as Y = 0.2126 * R + 0.7152 * G + 0.0722 * B, derived from Linear RGB to Y (Rec. 709 luminance formula). The second variant ω_2 incorporates the L* component from the CIELAB color space, which represents lightness, following a linearization step (sRGB → Linear RGB). In the example d is the Euclidian metric. The gradients are displayed in an inverted (negative) form without any normalization.

After applying morphological operations, the resulting image often contains a range of intensity values representing potential edges with varying strengths (as we can see, for instance, in Figure 2). By applying a threshold, weak or irrelevant responses (typically caused by texture, illumination changes, or noise) are suppressed, while strong transitions are preserved. Next, we will evaluate three different global thresholding methods that utilize gradient histograms. The choice of a global threshold for edge or contour detection based on the gradient histogram is motivated by its simplicity, robustness, and computational efficiency. A global threshold determines a single decision boundary for the entire image, which is particularly effective when illumination and contrast are relatively uniform. First variant that we use is based on simple valley analysis method or mode method [6]. Specifically, to determine the global threshold based on the histogram of one of morphological gradients, the algorithm follows these steps:

1. Histogram smoothing: The algorithm first smooths the histogram (using a Gaussian filter) to remove small fluctuations or noise, making the main intensity peaks more evident.

2. Find the main peak: The global maximum represents the most common intensity value (typically corresponding to the background or the dominant region in the image).

3. Search for a valley: After this main peak, the algorithm looks for a local minimum

(a "valley"); this usually lies between two classes of pixels (background vs. object).

4. Depth check: The valley is accepted only if it is significantly lower (less than 30% of the height of the main peak in implementation used here). This ensures it's a meaningful separation between two intensity clusters.

5. Fallback mechanism: If no clear valley is detected (for instance, if the image has no distinct bimodal distribution), the algorithm uses the percentile methods (p-tile method [sa]): finds the intensity value (or histogram bin) that corresponds to a given percentile of the total pixel distribution; for the examples in this paper, we use the 80th percentile of the intensity values.

The second method selected for determining the optimal threshold is the Otsu method [4], which maximizes the between-class variance, applied after gradient normalization.

The third approach for automatic threshold selection used in this paper is the Ng valley-emphasis method [3], which is also applied after gradient normalization.

For instance, in the case of ω_2 (the second grayscale conversion variant of the Lenna image), the simple valley yields a threshold of t = 117. The Otsu method yields a threshold of t = 36, while the valley-emphasis method produces t = 37 (d the Euclian metric). The corresponding (inverted) thresholded gradients, computed using the symmetric morphological gradient within the rough approximation framework, are presented in Figures 3 and 4.

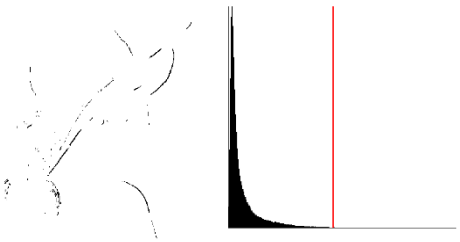

$g_r(\omega_2)$, r = 2 histogram
Threshold t = 117
Figure 3. (valley method)

$g_r(\omega_2)$, r = 2 histogram
Threshold t = 37
Figure 4. (valley emphasis method)

Let's consider a test image Figure 5 that contains several random geometric shapes. In the following examples d is the Euclidian metric.

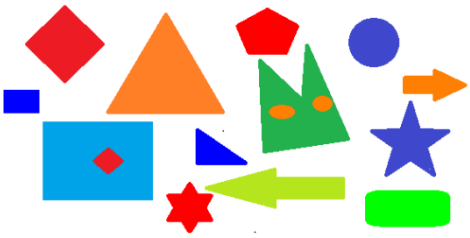

Figure 5. Test image (shapes)

Figure 6 illustrates the thresholded symmetric morphological gradients within the rough approximation context for the two variants of grayscale of test image in Figure 5 (at the top of the figure ω_1 is obtained using Rec. 709 luminance formula and at the bottom of the figure ω_2 is obtained using L*) using automatic threshold selection by: 1 – simple valley method, 2 – Otsu method and 3 – Ng valley-emphasis method.

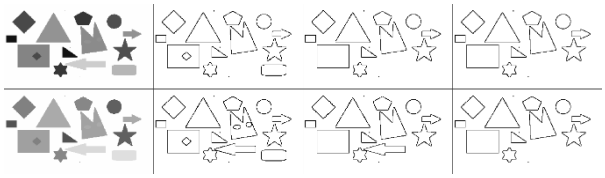

ω_i 1 (valley) 2 (Otsu) 3 (Ng)
Figure 6. Inverted thresholded $g_r(\omega_i)$, r = 2

Figure 7 displays the thresholded morphological gradients overlaid on images ω_1

and ω_2. The symmetric gradient is shown in red, the internal gradient in green, and the external gradient in blue. The threshold is determined using simple valley method, r = 2.

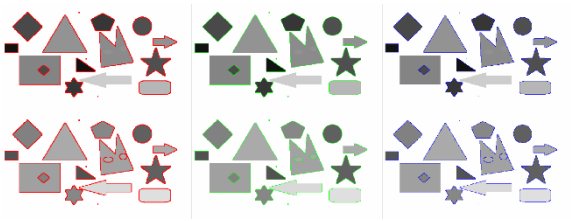

$g_r(\omega_i)$ $g_r^-(\omega_i)$ $g_r^+(\omega_i)$

Figure 7

In Figure 8, all thresholded gradients are displayed using the RGB color model: the symmetric gradient appears in the red channel, the internal gradient in green, and the external gradient in blue. Therefore, when all gradients detect the point as being on an edge (or contour), it is visualized using white. Points in magenta were detected by symmetric and external gradient, points in yellow by symmetric and internal gradients and points in cyan by internal and external gradients. The threshold is determined using simple valley method. At the top of the figure r = 5 and at the bottom r = 10.

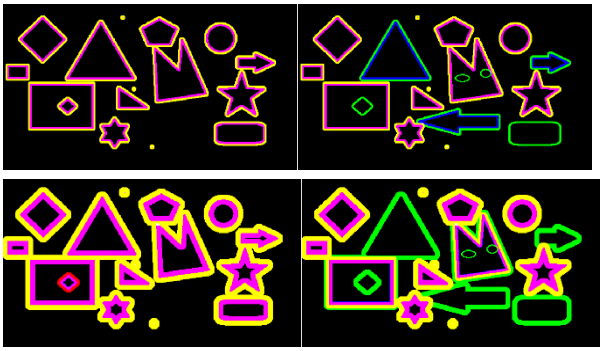

ω_1 ω_2

Figure 8. $g_r(\omega_i)R + g_r^-(\omega_i)G + g_r^+(\omega_i)B$

Similarly, in Figure 9 all all thresholded gradients are displayed using the RGB color model next to grayscale versions of the same images: (at the top of the figure ω_1 is obtained using Rec. 709 luminance formula and at the bottom of the figure ω_2 is obtained using L*) The threshold is determined using Ng valley emphasis method. The radius used in Figure 9 is r = 8.

ω_i $g_r(\omega_i)R+g_r^-(\omega_i)G+g_r^+(\omega_i)B$

Figure 9. Ng threshold, r = 8

3. COMPARISON OF GRADIENTS BASED ON ROUGH APPROXI - MATIONS WITH CLASSICAL MOR - PHO-LOGICAL GRADIENTS

Classical morphological gradient, computed through simple erosion and dilation operations, have been fundamental tools for edge detection and shape analysis due to their simplicity and computational efficiency. Let's us recall (and extend) their definition in our framework.

We denote by

$$\delta_r, \mathcal{E}_r: \mathcal{F}(X) \to \mathcal{F}(X)$$

the operators defined by

$$\delta_r(\omega)(x) = \sup\{\omega(s) \mid s \in L_r(x)\}$$

$$\mathcal{E}_r(\omega)(x) = \inf\{\omega(s) \mid s \in R_r(x)\}.$$

Let us note that if X is endowed with a group structure with the unit element denoted by 0 and the hemimetric d is translation invariant, then δ_r is the classical dilation operator with the structuring element $L_r(0)$, and $\mathcal{E}_r$ is the classical erosion operator with the structuring element $R_r(0)$. Although in the case where the hemimetric is not translation invariant these operators no longer represent the classical dilation and erosion, in this paper we agree to call them dilation and erosion. We note that if the hemimetric does not have the symmetry property the structuring element $L_r(0)$ for δ_r is different from the structuring element $R_r(0)$ for $\mathcal{E}_r$.

Since $x \in L_r(x)$ and $x \in R_r(x)$, for all ω in $\mathcal{F}(X)$, we have $\mathcal{E}_r(\omega) \leq \omega \leq \delta_r(\omega)$. Thus, we can define morphological gradients using δ_r, $\mathcal{E}_r$ even if the hemimetric d is not symmetric or not translation invariant:

$$\nabla_r(\omega) = \delta_r(\omega) - \mathcal{E}_r(\omega)$$
$$\nabla_r^-(\omega) = \omega - \mathcal{E}_r(\omega)$$
$$\nabla_r^+(\omega) = \delta_r(\omega) - \omega.$$

In the following, we will call ∇_r, ∇_r^-, ∇_r^+ classical symmetric morphological gradient, classical internal morphological gradient, and classical external morphological gradient, respectively.

To facilitate a comparative analysis between the gradients derived from the rough approximation framework and the traditional morphological gradients (utilizing various automated thresholding techniques), we introduce a visualization approach based on superimposing the resulting gradient images. Specifically, for each input image, both the new gradient and the classical gradient are computed and overlaid. Points corresponding to contours or edges identified by the new gradient are highlighted in red, those from the classical gradient are shown in green, and regions where both gradients agree are displayed in black.

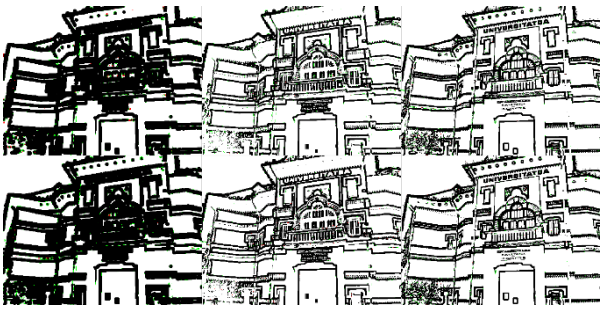

$g_r(\omega i) + \nabla_r(\omega_i)\, g_r^-(\omega_i) + \nabla_r^-(\omega_i)\; g_r^+(\omega_i) + \nabla_r^+(\omega)$

Figure 10. Otsu threshold, r = 7

At the top of Figure 10 the figure ω_1 is obtained using Rec. 709 luminance formula and at the bottom of the figure ω_2 is obtained using L*. The threshold is determined using Otsu method. The radius used in Figure 10 is r = 7.

4. MULTISCALE REGULARIZED GRADIENTS

We also propose a multiscale regularized gradient in a similar way with the algorithm presented in [b] based on the regularized gradient [ri]. Let us consider a sequence of n positive real numbers $\rho = (r_1, r_2, \ldots, r_n)$ such that

$$r_1 < r_2 < \ldots < r_n$$

Algorithm for computing the multiscale regularized gradient $g(\omega)$ using the scale ρ

1. compute $g_{r_1}(\omega) \leftarrow \overline{App}^{r_1}(\omega) - \underline{App}^{r_1}(\omega)$
2. $g(\omega) \leftarrow g_{r_1}(\omega)$
3. for i = 2 to n do
   //compute "regularized" gradient at scale r_i
   $g_{r_i}(\omega) \leftarrow \overline{App}^{r_i}(\omega) - \underline{App}^{r_i}(\omega)$
   $g_{r_i}(\omega) \leftarrow g_{r_i}(\omega) - \overline{App}^{r_i} \circ \underline{App}^{r_i}(g_{r_i}(\omega))$
   $g_{r_i}(\omega) \leftarrow \underline{App}^{r_i - 1}(g_{r_i}(\omega))$
   //update $g(\omega)$
   $g(\omega) \leftarrow \sup\{g(\omega), g_{r_i}(\omega)\}$
   end for

Figure 11

In Figure 11 we compare the results of the preceding algorithm for $r_i = 1.5 + I$, applied to the image ω_2 (obtained using L*, see Figure 10) for n = 2 and n = 8. The threshold employed is determined by selecting the minimum value among the thresholds for symmetric, internal, and external gradients associated with $g_n(\omega_2)$ all

computed using Otsu method (n= 2 versus n = 8). The images $g_2(\omega_2)$ and $g_8(\omega_2)$ are overlaid as in Section 3. Points displayed in green are points added by $g_8(\omega_2)$.

5. CONCLUSION

In this paper, we defined new variants of the morphological gradient constructed from the neighborhood-controlled fuzzy upper and lower rough approximation operators (introduced in [2]), leveraging their extensive and anti-extensive nature as a natural analogue to dilation and erosion. To assess how these fuzzy rough gradients compare to their classical counterparts, we employed a comparative visualization approach based on the superposition of resulting gradient images. Our C implementations, using SDL3 for efficient pixel access, enabled a controlled and reproducible evaluation framework.

The experimental results indicate that the proposed operators behave in a broadly similar manner to the classical morphological gradient, while exhibiting a tendency to produce thinner and more localized edge structures (although more tests are needed). This behavior suggests that the fuzzy rough formulations may offer advantages in contexts where fine-grained or uncertainty-sensitive edge delineation is desirable. However, our present study is limited to the Euclidean distance, chosen deliberately to maintain exact comparability with the classical operators, and relies on a global automatic thresholding scheme.

Future work will address these limitations by incorporating hemimetrics tailored to local intensity variations, thereby allowing the fuzzy rough operators to better accommodate heterogeneous or textured regions. Such an extension is expected to further reveal the potential of these operators as flexible, context-adaptive tools within the broader domain of morphological image analysis.

REFERENCES

[1] J.-C. Bricola, M. Bilodeau and S. Beucher. *A multi-scale and morphological gradient preserving contrast*, 14th International Congress for Stereology and Image Analysis, Jul 2015, Liege, Belgium. hal-01158715v2

[2] X. Han, W. Yao, C.-J. Zhou, *A fuzzy topological model of hemimetric-based fuzzy rough set and some applications to digital image processing*, Topology and its Applications, 367 (2025), 109327.

[3] H. Ng, *Automatic thresholding for defect detection*, Pattern Recognition Letters, 27 (2006), 1644 - 1649.

[4] N. Otsu, *A threshold selection method from gray-level histograms*, IEEE Transactions on Systems Man Cybernet, SMC-9 (1) (1979), 62–66.

[5] J. F Rivest, P. Soille and S. Beucher, *Morphological gradients*. In SPIE/IS&T 1992 Symposium on Electronic Imaging: Science and Technology (pp. 139-150). International Society for Optics and Photonics, 1992.

[6] P.K Sahoo, S Soltani and A.K.C Wong, *A survey of thresholding techniques*, Computer Vision, Graphics, and Image Processing, 41 (2) (1988), 233-260.

[7] F. Y. Shih, *Image Processing and Mathematical Morphology Fundamentals and Applications*, CRC Press, 2009.

[8] D. Yang, B. Peng, Z. Al-Huda, A. Malik and D. Zhai, *An overview of edge and object contour detection*, Neurocomputing, 488 (2022), 470-493.

[9] W. Yao, G. Zhang, C.-J. Zhou, *Real-valued hemimetric-based fuzzy rough sets and an application to contour extraction of digital surfaces*, Fuzzy Sets and Systems 459 (2023), 201–219.